Background Reading Report

by

Team 3: Tatiana Kashtanova, Samuel Ydenberg

Project Summary & Background Reading Selection

Radiation therapy (RT) is a type of cancer treatment where a high radiation dose is delivered to the tumor while minimizing the exposure of the surrounding healthy tissue. The procedures ensuring the precise and safe delivery of radiotherapeutic dose are called Quality Assurance (QA)[1,2] and govern treatment planning, treatment verification, and treatment delivery. Our project focuses on the treatment verification aspect of QA. The objective of our project is to implement a new QA method for RT using scattered x-ray registration[3] which would allow for real-time external monitoring of the delivered dose deposition. The main milestones of the project are 1) to implement a photon counting detector for scattered photons registration within the gDPM simulation package[4,5] developed by our mentors, 2) to relate the detector signal to the depth-dose profile, 3) to verify the simulation work by comparing it with physical measurements.

When doing literature search, we found out that the project idea was not as novel as we thought. It was first proposed and implemented by Portuguese researchers about a decade ago. In this background reading report, we summarize two papers on their work titled “Dose-free monitoring of radiotherapy treatments with scattered photons”[6,7]. The first paper with a subtitle “Concept and simulation study”[6] discusses the rationale behind and composition of the proposed system for external monitoring of depth-dose distribution in radiotherapy sessions as well as the results of the conducted simulation experiments. The second paper with a subtitle “First experimental results at a 6-MV Linac”[7] discusses the challenges of implementing the system, previously constructed in the simulation environment, in the physical world, the developed solutions to the problems, and the results of the physical measurements.

Paper 1. Relevance

The first paper is titled "Dose-free monitoring of radiotherapy treatments with scattered photons: Concept and simulation study". The paper is relevant to our project because the authors implemented the same method of monitoring radiotherapy dose deposition but used a different simulation environment and more complex phantoms. Thus, the authors used the Geant4 simulation toolkit[8] while we are working with the gDPM; the authors used heterogeneous phantoms while we initially planned to use only homogeneous ones.

Paper 1. Introduction

During RT sessions, the greatest challenges in delivering the prescribed dose precisely are patient mispositioning, organ movements, and anatomical morphological changes (e.g., tumor shrinkage/growth, tissue inflammation, filling of cavities with mucus, etc.), all of which may result in tumor underdose and organs-at risk overdose. The current solutions include image-guided radiation therapy (IGRT) and adaptive radiotherapy (ART) where physicians use imaging to detect deviations from the initial planning and make the corresponding adjustments. The main disadvantage of the methods is extra-dosage. That is where the authors came in with an idea to develop a gamma-camera-like system allowing real time depth-dose verification without extra-dosage using scattered photon registration.

Paper 1. Concept

Figure 1 depicts the proposed dose monitoring system in a clinical RT environment. Here, a patient is lying on a couch. A photon beam comes from the head of a linear accelerator (Linac). A photon-counting detector with a high-energy collimator in front of it is positioned above the patient head at a right angle with the beam direction. The detector accepts photons scattered perpendicularly to the beam. The researchers are interested in two questions: (1) if the scattered photons correlate with the deposited dose; and (2) if edema (swelling) could be detected with such a system.

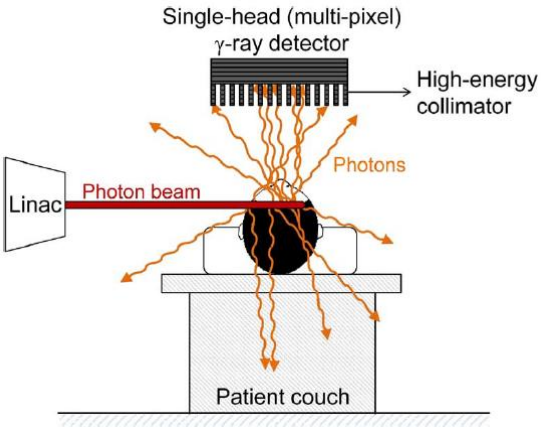

Figure 1: Proposed dose monitoring system in a clinical RT environment[6]

Paper 1. Materials and Methods

Using the Geant4 simulation toolkit, the authors constructed two cylindrical phantoms filled with water and having an air cavity and bone (tumor) inside. The left phantom in Figure 2 represents a normal case where the air cavity is positioned directly next to the bone. The right phantom in Figure 2 represents a case with a morphological alteration: the size of the air cavity is reduced, and the space is filled with water (mucus).

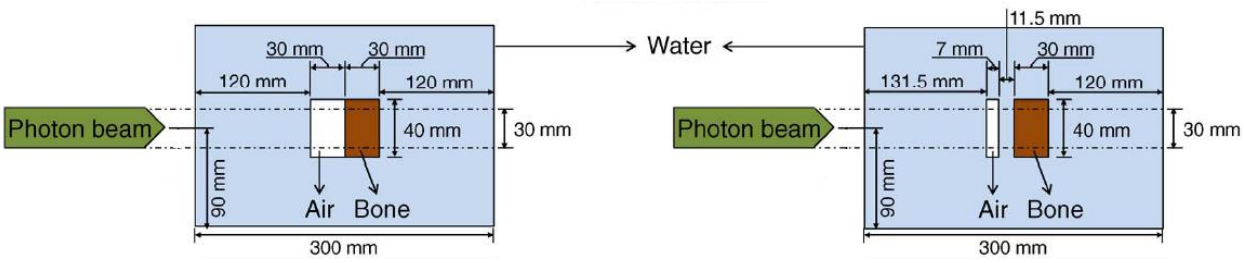

Figure 2: Simulated phantoms[6]

The simulated photon beam spectra had endpoint energies of 6 MV and 18 MV which were selected to mimic the ones typically used to treat head-and-neck and lung tumors, respectively. The simulated beams hit the phantoms with no divergence. The interactions of the radiation with the matter were governed by the chosen "electromagnetic processes" physics list in Geant4.

To register only those photons that scattered at approximately right angles ($89.3° \leq \Theta \leq 90.7°$) to the beam direction and possessed a certain amount of energy, the authors also constructed a multi-hole collimator with hexagonal holes in the simulation environment. The collimator was made of

lead and had a rectangular parallelepiped shape with a length of 300 mm and a height of 150 mm. Table 1 shows other collimator geometric parameters defined to collimate photons with specific nominal energies. Here, the variable "septa thickness" means the distance between two adjacent collimator holes, "face-to-face distance" means the distance between two opposite faces of a hexagonal hole, and "collimator thickness" means the collimator width. The collimator front face (the side facing the phantom) was positioned at 280 mm from the central axis of the beam.

Table 1. Computed collimator geometrical parameters[6]

Energy (keV)	Collimator thickness (mm)	Septa thickness (mm)	Face-to-face distance (mm)
200	45.912	0.12763	0.96548
300	80.811	0.31217	1.5349
400	116.99	0.52669	2.0196
500	151.40	0.73275	2.4051
600	182.93	0.91566	2.7080
800	237.43	1.2104	3.1445

Paper 1. Results & Discussion

First, the authors validated the physics list chosen in the simulation toolkit by comparing the simulated depth-dose profile with published data on a case where a 6-MV photon beam was applied to a cylindrical homogeneous water phantom. The published and simulated depth-dose profiles were visually well correlated, with a small difference near the entrance to the phantom.

Then, the authors conducted different experiments. We will focus on the one most related to our project. Here, the authors used a plane photon-counting detector with the multi-hole collimator placed in front of it to register photons carrying a specific nominal energy. The top plot in Figure 3 shows the two-dimensional distribution of photon counts hitting the plane detector sensor in the presence of the collimator designed for a nominal photon energy of 600 keV. The simulated photon beam had the endpoint energy of 6 MV and the irradiated phantom had the morphological alteration. The bottom plot in Figure 3 shows the comparison between the simulated depth-dose profile (dashed curve) and the corresponding profile of the scattered photons (solid curve) which is computed as the integral of the number of photon counts divided by the average dose delivered to the bone (tumor). While there is a difference between the two profiles, especially in the bone

area and near the entrance to the phantom, the authors claim that the registered scattered photons respond well to the heterogeneity of the phantom including the air cavity reduction.

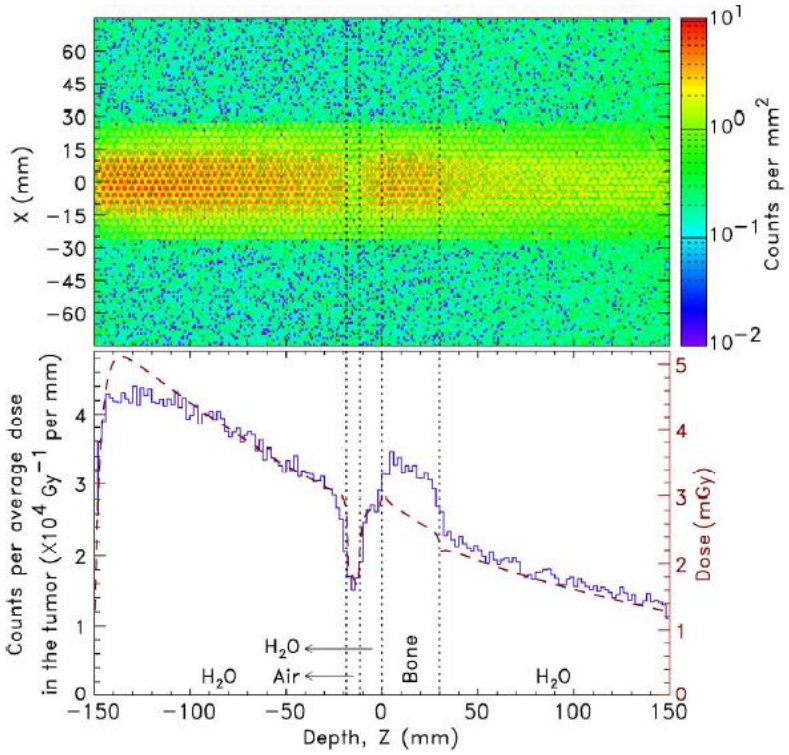

Fig. 3. Two-dimensional distribution of photon counts hitting the detector sensor (top); Comparison between the simulated depth-dose profile and collimated for 600 keV photon profile (bottom)[6]

Table 2 presents the results of the statistical analysis of the relation between the dose data and counted photons detected with each energy collimator. Here, RMSE stands for the root mean square error. The authors conclude that the collimator designed for a nominal photon energy of 600 keV gives the best dose-correlated results.

Table 2. Statistical analysis of the relation between the dose data and counted photons[6]

Energy (keV)	RMSE	Correlation (R) between dose and detected photons profiles
200	10813.15	-0.9430
300	2143.04	-0.9029
400	319.24	-0.4749
500	119.91	0.9308
600	110.78	0.9442
800	94.03	0.9324

Paper 1. Critical Review

The pros of the paper: 1) It is a great implementation of our project (minimum and expected deliverables); 2) The authors considered heterogenous phantoms; 3) The authors validated the physics list chosen in the simulation toolkit; 4) The authors explored the effect of different collimator energy thresholds on the correlation between the dose data and detected photon counts.

The cons of the paper: 1) When validating the physics list, the authors compared the simulated and published depth-dose profiles only visually; 2) The authors did not mention the dimensions of the plane detector and its sensor area in the discussed experiment; 3) The authors did not elaborate on potential reasons of the difference between the simulated depth-dose profile and the profile of counted photons in the bone area and near the entrance to the phantom; 4) Comparison of the simulation results with physical measurements would be beneficial.

Key takeaways: 1) We learned that our method of monitoring radiotherapy dose deposition was not novel; 2) In our project, we should also consider the use of heterogenous phantoms and perhaps real computed tomography scans; 3) We should explore different collimator energy thresholds while starting with the ones discussed in the paper; 4) We learned that no complicated mathematics might be needed to relate the detector signal to the deposited dose.

Paper 2. Relevance

The second paper is titled “Dose-free monitoring of radiotherapy treatments with scattered photons: First experimental results at a 6-MV Linac” [2]. The paper is relevant to our project because the authors implemented the same QA method in a real clinical environment but using a different photon counting detector (a single-pixel photomultiplier tube vs. our dual-energy XC-THOR) and a more complex phantom. The paper complements the previously discussed work by attempting to build the simulated system in the physical world.

Paper 2. Introduction

The main challenge of implementing the simulated system in a physical environment is the so-called out-of-field flux (Figure 4, left) which represents a background flow of photons and other particles coming out from the Linac head alongside the produced photon beam. Not only does the out-of-field flux introduce extra radiation around the desired target (Figure 4, right), it also gets mixed with the scattered photons correlated with the prescribed dose, thus impairing the detector sensor readings which, in turn, causes incorrect conclusions on the depth-dose deposition.

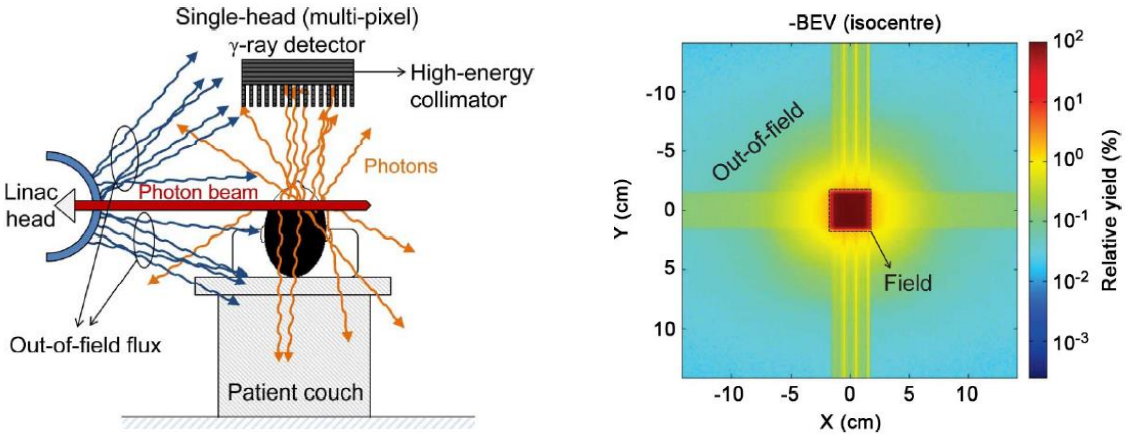

Fig. 4. Out-of-field flux: The concept (left); Beam’s eye view of a particle flux coming to a 3 cm x 3 cm filed together with out-of-field radiation (right)[7]

In this paper, the authors describe their RTmon (RT monitoring) system allowing to mitigate the impact of out-of-field flux and register the desired scattered photons. They also present the first physical measurements and the results of reconstructing the delivered depth-dose profile based on the recorded detector signal.

Paper 2. Materials and Methods

Figure 5 depicts the RTmon experimental setup. The 6-MV photon beam has 30 mm x 30 mm filed size at the isocenter and is delivered by a Siemens ONCOR Avant-Garde Linac. The phantom is made of polymethylmethacrylate (PMMA) and has a cylindrical shape with 180-mm diameter and 300-mm length. In the phantom center, there is a cylindrical air cavity with 30-mm diameter and 20-mm length. The collimator is made of iron-Cerrobend™; its height is 149 mm, the diameter of the inner-hole is 6 mm. The collimator is positioned at the right angle to the beam direction at 110 mm from the phantom. The scintillator crystal (used for x-ray conversion) is made of four cerium-doped lutetium yttrium oxyorthosilicate crystals wrapped together in Teflon tape. Each crystal is 20-mm length and 2 mm x 2 mm front face. The front face of the crystals' combination is 4 mm x 4 mm. The scintillator crystal is inserted into the collimator hole and its front face is attached to the photocathode of a photomultiplier tube (PMT). The tube itself is surrounded by a hollow iron cylinder (20-mm wall thickness) for radiation protection. This single-pixel collimated detection system registers photons scattered in the phantom center at $89.3° \leq \Theta \leq 90.7°$ angles.

To collect at least eight samples per pulse during the detection of the scintillation light from the crystal, the PMT output signal is shaped using the readout electronics chain which moves the PMT signal sequentially through a Canberra pre-amplifier (model 1130-4), a Canberra spectroscopy amplifier (model 2020), and a self-programmed PicoScope oscilloscope (model 2203).

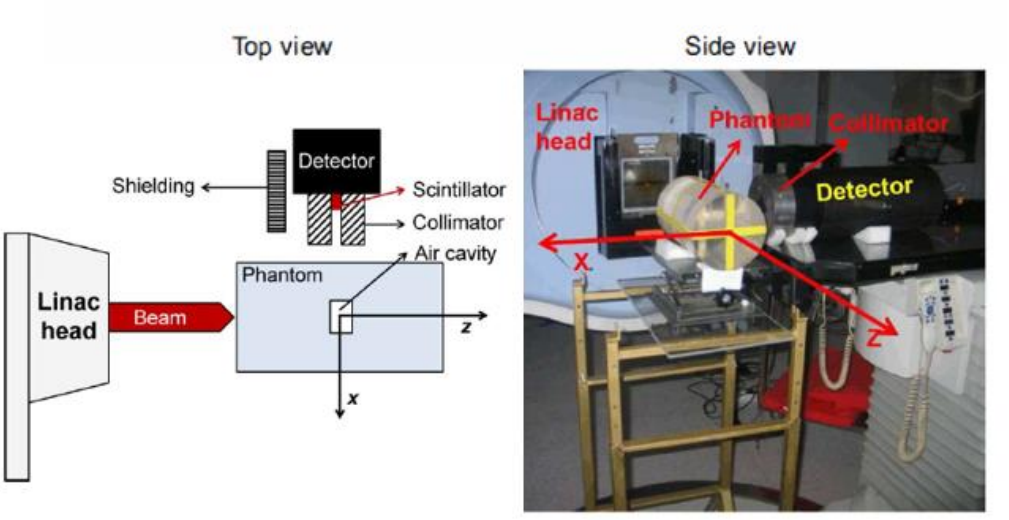

Fig. 5. RTmon experimental setup[7]

When attempting to mitigate out-of-field Linac flux, the authors explored the impact of 1) the positioning of a 60-mm thickness Cerrobend^{TM} shielding block between the Linac head and the detector (Figures 5,6); 2) the positioning of a tungsten block in front of the inner hole of the collimator; 3) the positioning of the detector at 70 mm, 110 mm, and 150 mm from the phantom surface which corresponded to the placement of the detector at x = -160 mm, -200 mm, and -240 mm in the coordinate system, respectively (Figure 6). Longitudinal (along z-axis) detector signal scans were obtained by moving the detector from the position z = -120 mm to the position z = 120 mm with a 20-mm incremental step (Figure 6).

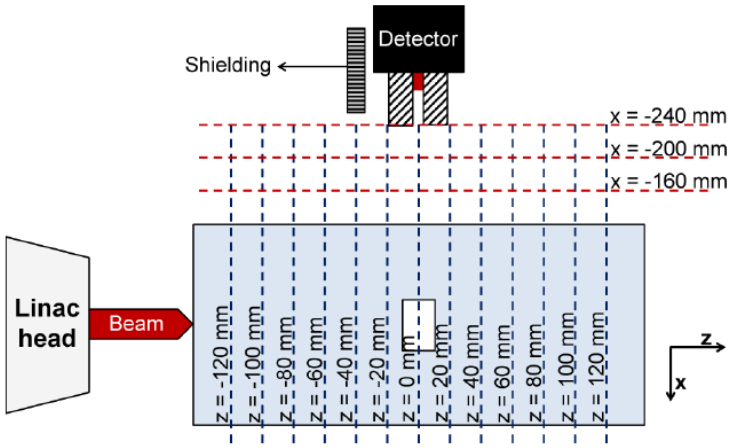

Fig. 6. Out-of-field flux mitigation experiments[7]

Paper 2. Results & Discussion

In the first study on the out-of-field flux mitigation, the authors assessed the shielding efficiency of the Cerrobend^{TM} block positioned between the Linac head and the detector. The left plot in Figure 7 shows the recorded pulse height spectra in the presence of the block (blue) and in its absence (red). The black solid and dashed lines represent the Gaussian fits obtained for the spectra. The authors claim that the shielding provides a 57% reduction in the background signal.

In the second study, the authors placed a tungsten block in front of the collimator inner hole in addition to the Cerrobend^{TM} block positioned between the Linac head and the detector. The rationale behind the experiment was in suppressing the signal from radiation scattered in the phantom so that the detector readings corresponded mainly to the background flux. The right plot in Figure 7 shows the registered pulse height spectra with (blue) and without (red) the tungsten

shielding when the detector was located at z = -120 mm; the black lines show the Gaussian fits. The authors note that the shielding reduces the physical signal arising from the phantom.

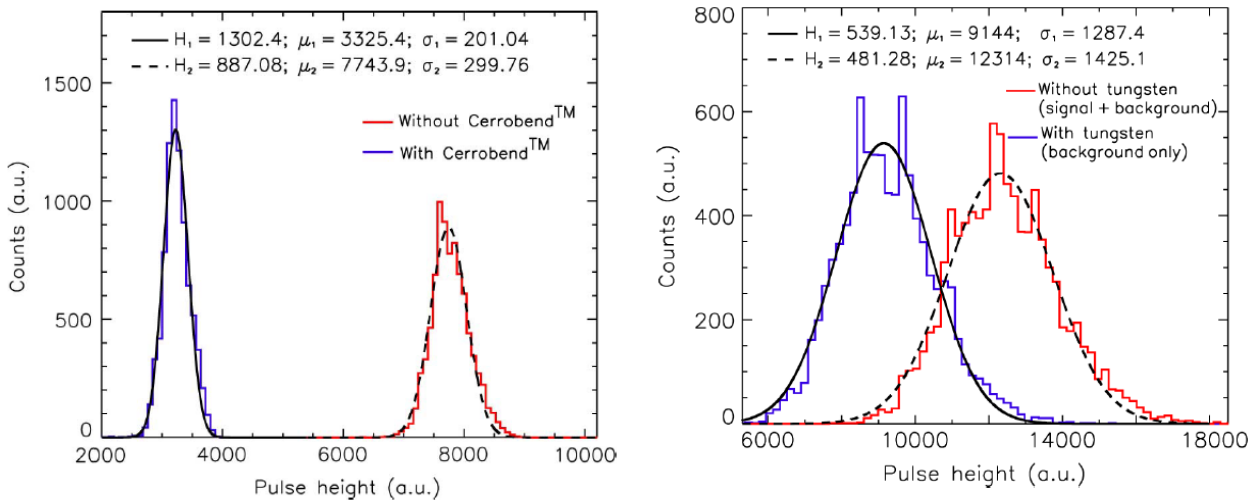

Fig. 7. Pulse height spectra obtained: with and without Cerrobend™ shielding (left); with and without tungsten block in the presence of Cerrobend™ shielding (right)[7]

In the next experiment, the authors recorded a longitudinal scan by moving the detector along the z-axis with a 20-mm incremental step. At each position, the authors obtained the corresponding pulse height spectrum with the Gaussian amplitude. The experiment was repeated in the presence of the tungsten block and Cerrobend™ shielding where mainly the background flux was measured and in the absence of the tungsten block where both the scattered photon signal and the background flux were recorded. Then, the authors subtracted the background pulse height spectrum from the signal + background pulse height spectrum to obtain a pulse height spectrum free of the background noise. Figure 8 (left) shows the subtraction result when the detector was positioned at x = -200 mm. The red curve represents the simulated depth-dose profile which is shown in arbitrary units and visually adjusted to the subtracted pulse height spectrum. The error bars for the signal + background, only background, and the differential signal are around 0.2% and not visible.

Finally, the authors repeated the background subtraction experiment while positioning the detector at three different x-values (-160 mm, -200 mm, and -240 mm). Figure 8 (right) depicts the results. The authors say that the error bars are no more than 0.4% for all x-locations and that the detector position at x = -200 mm gives the best agreement with the simulated depth-dose data.

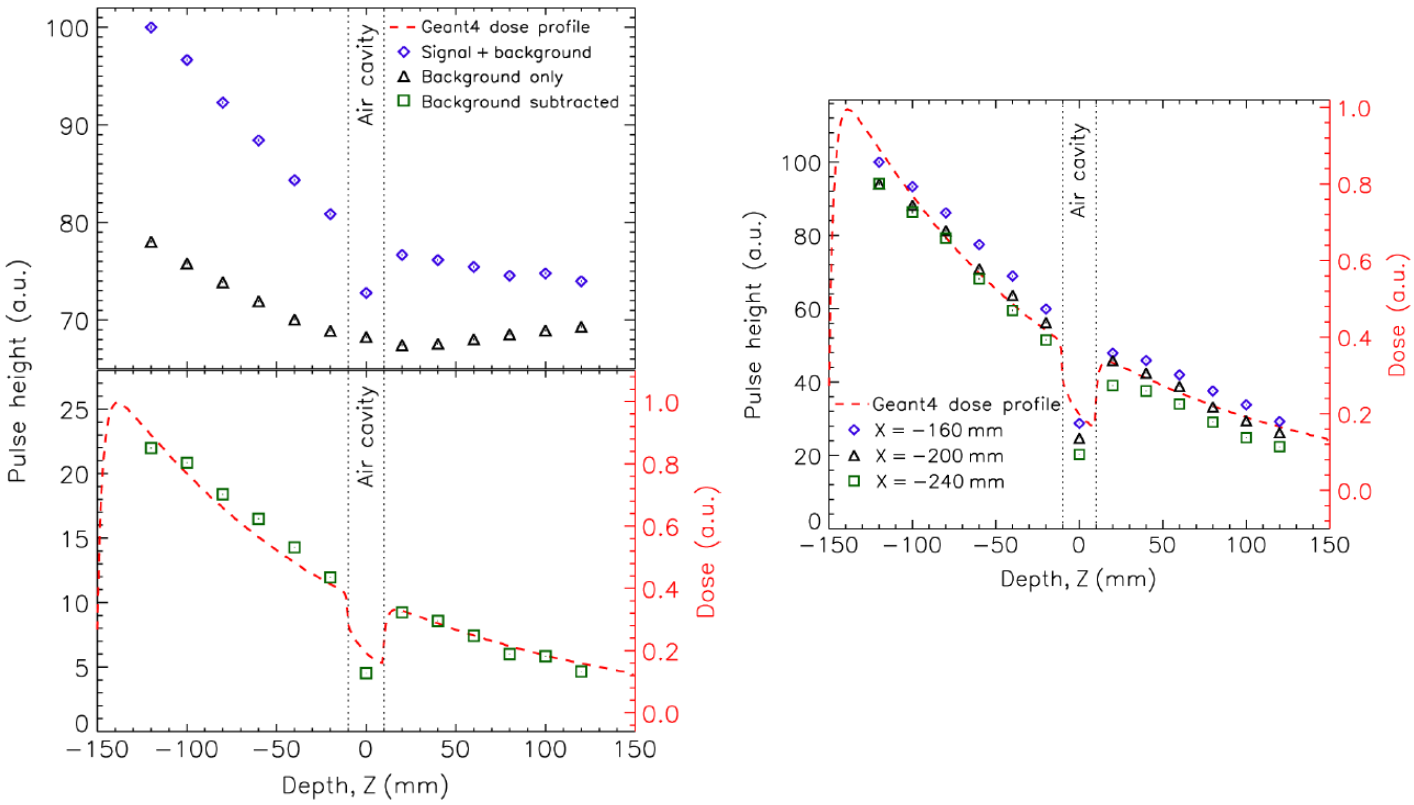

Fig. 8. Scan profiles along the phantom depth: the background subtraction when the detector is positioned at x = -200mm (left); Background-free measurements for different detector positions (right)[7]

Paper 2. Critical Review

The pros of the paper: 1) It is a great implementation of our project (maximum deliverable); 2) It is built on the previously discussed paper which makes it easy to connect the simulation and experimental studies 3) It describes methods for dealing with out-of-field flux.

The cons of the paper: 1) The authors used a single-pixel collimated detector which has a poor resolution; 2) The comparison of the pulse height data with the simulated depth-dose profile in arbitrary units which is also somehow visually adjusted is not sufficient for inferring the exact delivered dose deposition.

Key takeaways: 1) We learned that the physical experiments might be more challenging than we initially expected; 2) The presented research findings will assist us in positioning the detector and mitigating the out-of-field flux in our physical experiments.

Conclusion

While the discussed papers show that our project idea is not as novel as we initially thought, we will use the research findings to try to produce a more clinically beneficial work. Thus, at first, we will attempt to achieve a more precise detector signal by a) experimenting with the detector and shielding positioning as well as with the collimator photon energy thresholds starting with the values suggested by the authors; b) using a dual-energy XC-THOR detector which has a higher resolution. Then, we will test our work on different heterogeneous phantoms and, perhaps, actual computed tomography scans to mimic real-life clinical scenarios.

References

1. World Health Organization. (1988). Quality Assurance in Radiotherapy: a Guide Prepared Following a Workshop Held at Schloss Reisensburg, Federal Republic of Germany, 3-7 December1984. Geneva
2. Glide-Hurst, C.K., & Chetty, I.J. (2014). Improving radiotherapy planning, delivery accuracy, and normal tissue sparing using cutting edge technologies. *Journal of Thoracic Disease*, *6*(4), p.303–318
3. Jia, X. (2023). Quality assurance of radiotherapy treatment using scattered x-ray. Presentation slides for CIS II
4. Jia, X. & Jiang, S.B. (2011). gDPM v2.0. A GPU-based Monte Carlo simulation package for radiotherapy dose calculation. The Center for Advanced Radiotherapy Technologies (CART), UCSD
5. Jia, X., Ziegenhein, P., & Jiang, S. B. (2014). GPU-based high-performance computing for radiation therapy. *Physics in Medicine and Biology*, *59*(4), p. R151–R182
6. Cunha, M., et al. (2013). Dose-free monitoring of radiotherapy treatments with scattered photons: Concept and simulation study. *IEEE Transactions on Nuclear Science, 60*(4), p. 3119-3126
7. Simões, H., et al. (2013). Dose-free monitoring of radiotherapy treatments with scattered photons: First experimental results at a 6-MV Linac. *IEEE Transactions on Nuclear Science, 60*(4), p. 3110-3118
8. Geant4 (n.d.). A simulation toolkit. https://geant4.web.cern.ch/